

Spatial Identification of Key Alteration Minerals Using ASTER and Landsat 8 Data in a Heavily Vegetated Tropical Area

Kayvan Ghasemi¹ · Biswajeet Pradhan¹  · Ratiranjana Jena¹

Received: 9 June 2016 / Accepted: 8 May 2018 / Published online: 23 May 2018
© Indian Society of Remote Sensing 2018

Abstract

The Central Gold Belt (CGB) of Malaysia is a major host to gold deposits. Penjom, Raub, Selising and Buffalo reef are major gold mines in CGB. The study area, Selinsing gold mine, is located at the northwest of Pahang province on the lineament known as the Raub Bentong Suture. Presence of dense vegetation and cloud cover in tropical regions are main obstacles in alteration mapping using satellite imageries. In this study, Landsat 8 and ASTER level 1B images were used to map clay minerals and quartz rich zones at Selinsing gold mine and surrounding areas. Direct principal component analysis (DPCA), matched filtering (MF) and band ratio were the effective methods used in this study. High concentration of clay minerals was detected using band ratio 6/7, DPC2 and MF and ratio 14/12 was carried out to highlight quartz rich zones. The results of image processing methods were verified by in situ inspection and X-ray diffraction analyses. The results show that, in spite of limited bedrock exposure, the known gold prospects and potential areas of mineralization can be recognized by the methods employed in this study.

Keywords Minerals mapping · GIS · LANDSAT 8 · ASTER · Remote sensing

Introduction

Malaysia had already established itself as one of the important gold producers long before the development of the great gold-fields in South Africa and Australia. Prior to the Portuguese conquest of Malacca in 1511, the country was known as the “Aurea Chesonese” or “Golden Peninsular”. During the British reign between 1880s and 1940s, major gold production generally came from the state of Pahang, Kelantan and Negeri Sembilan. During this booming period, Raub, Selinsing, Kechau-Tui, Katok Batu, Penjom and Batu Bersawah goldfields were the important underground lode gold mines within the CGB (Chu and Singh 1986; Iswadi et al. 2009; Makoundi 2012). The study area, Selinsing Gold Mine (Fig. 1), is located at Bukit Selinsing Koyan, northwest of Pahang, approximately 65 km north of Raub on the lineament known as the Raub

Bentong Suture. Pahang is the largest gold producing state in Malaysia (Glacken et al. 2006). A general central coordinate for the Selinsing mine is approximately 4°15'0"N latitude, 101°47'10"E longitude.

Remote sensing data can provide global information of the Earth's surface and important data for evaluation of regional areas for mineral resources mapping in the early stage of exploration (Yajima 2014). Numerous studies using remotely sensed data have been demonstrated the feasibility of mapping alteration zones in arid and semi-arid areas (Salisbury et al. 1994; Harris et al. 1998; Crosta et al. 1998; Ducart et al. 2006; Moore et al. 2008; Molan et al. 2014; Pour and Hashim 2011, 2015). However, in heavily vegetated regions, mapping alteration zones using remote sensing is challenging due to the fact that spectral signatures received by sensor are mostly affected by vegetation (Almeida-Filho and Vitorello 1996; Galvao et al. 2005; Pour et al. 2013; Pour and Hashim 2014). Some of the examples of alteration mapping using remote sensing imageries are given below.

Almeida-Filho and Vitorello (1996) combined Landsat TM images with a high resolution aerial photograph via

✉ Biswajeet Pradhan
biswajeet24@gmail.com; Biswajeet.Pradhan@uts.edu.au

¹ School of Systems, Management and Leadership, Faculty of Engineering and Information Technology, University of Technology Sydney, Ultimo, NSW, Australia

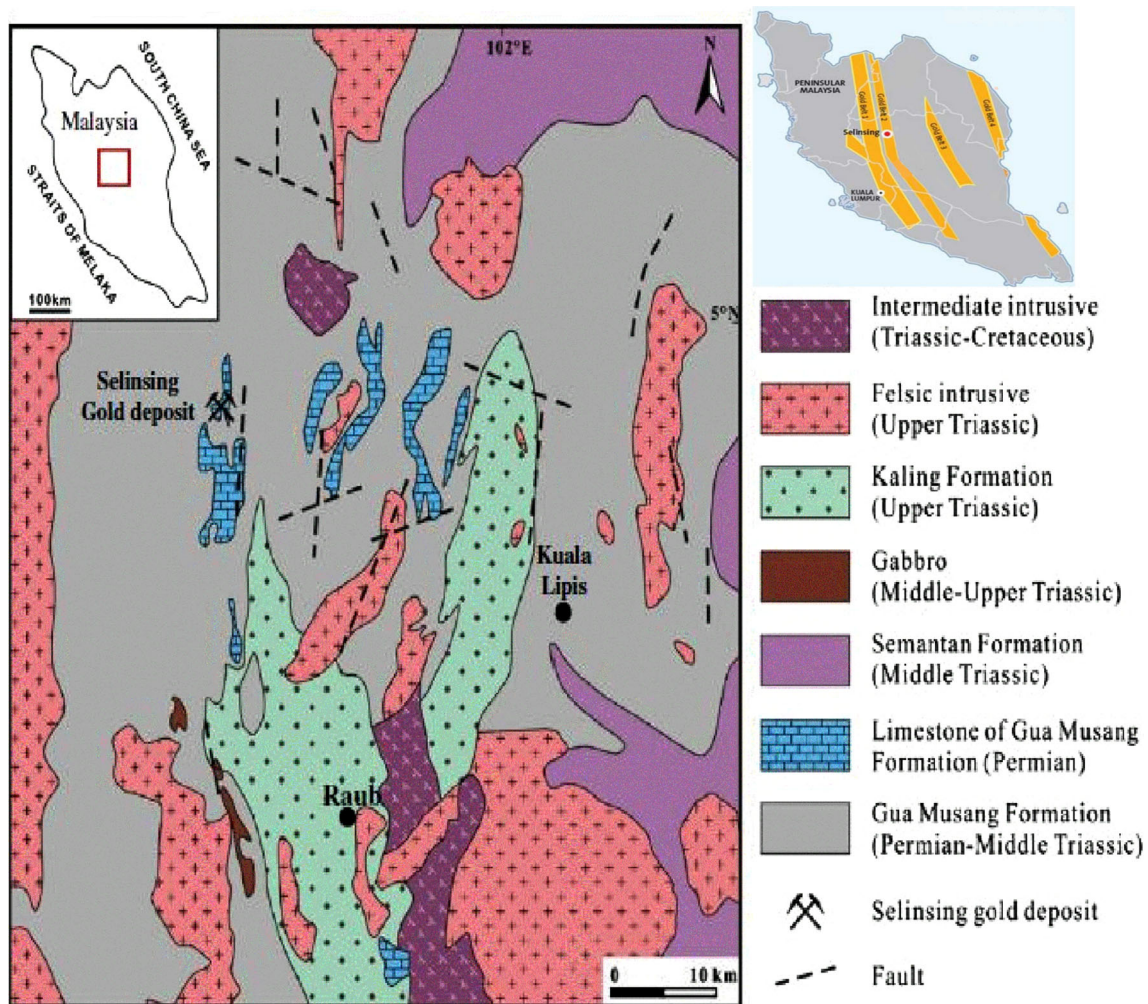


Fig. 1 Study area showing Selinsing geological map with gold belts (after Lee and Sallehuddin 1990)

HIS technique and mapped hydrothermal altered rocks in central Brazil using band combination. Pour et al. (2013) applied DPCA and Linear Spectral Unmixing (LSU) to Landsat ETM⁺ and Hyperin data respectively and successfully mapped clay and Iron oxide zones at Bau gold field, Malaysia. Pour and Hashim (2014) used ASTER data for mapping alteration zones in the eastern part of the Central Belt of Peninsular Malaysia. Alunite, kaolinite, Carbonate, Quartz and OH bearing-altered indices were utilized to produce alteration and lithological maps. Volesky et al. (2003) applied band ratio on ASTER bands. They mapped propylitic alteration and gossans in the Neoproterozoic Wadi Bidah in Saudi Arabia. Rowan et al. (2003) used matched-filtering to discriminate hydrothermally altered and unaltered rocks in Nevada, USA using ASTER data. Their results showed that ASTER VNIR and SWIR can provide accurate spectral information for highlighting the main hydrothermal alteration zones. Moore et al. (2008) utilized ASTER Level 1A data to highlight alteration zones. They discriminated argillic and silicic

alteration using SPCA, relative absorption band-depth (RBD) and matched-filtering (MF). Boloki and Poormirzaee (2010) examined Selective Principal Component Analysis (SPCA) on ASTER data to map key alteration minerals in Siyahrud, Iran. They were able to map alteration minerals in the region using 4 SPCA bands. Pour and Hashim (2011) assessed the feasibility of the ASTER data to map alteration zone in two copper mining districts called Sarcheshmeh and Meiduk in Iran. They discriminated iron oxides and OH-bearing minerals using PCA, minimum noise fraction (MNF) and band ratio. In another paper, Hosseinjani Zadeh et al. (2014) identified muscovite, illite, kaolinite, goethite, hematite and chlorite using EO-1 Hyperion data. Mixture tuned matched filtering (MTMF) was the method that they applied. Oskouei and Babakan (2016) used Hyperion data to map Kaolinite and Silicified zones at Lahroud, NW Iran. MF and MTMF techniques were utilized and based on their results, it is clear that MTMF worked better than MF. Feizi et al. (2016) introduced some new prospects of Au using alteration maps and

geochemical data at Shishe Botagh, NW of Iran. They applied band ratio, MNF and SAM to ASTER data and successfully mapped Iron oxide, propylitic and phyllic alteration and Silica in the study area.

Based on the above literature review, in vegetated areas band ratio cannot work perfectly for mapping hydroxide bearing minerals due to the similarity between spectral signature of these minerals and vegetation. However DPCA could work perfectly in highly vegetated areas. In arid and semi-arid regions, PCA, SPCA and Hyperspectral image processing methods such as MF and MFMF can successfully map alteration zones. The aim of this study is to evaluate the feasibility of conventional image processing methods including band ratio, DPCA and MF to map key alteration minerals in heavily vegetated areas using Landsat 8 and ASTER thermal bands.

Study Area

Peninsular Malaysia has traditionally been divided into three north–south-trending zones based on differences of stratigraphy, mineralization and structure. These zones have been variously referred as the Western, Central and Eastern “Belts” (Fig. 1) “Zones” or “Domains”. The Peninsula is made up of two blocks, Sibumasu (Continental block derived from Gondwana) and Indochina (Arc terranes derived from South china or Indochina) blocks (Metcalf 1986, 1988, 2000). CGB is bounded by the Bentong-Raub Suture Zone to the west and the Lebir Fault Zone to the East (Campi et al. 2002). The Central Belt consists mainly of Permo Triassic, a low-grade metasediments, deep to shallow marine clastic sediments and limestone with abundant intermediate to acid volcanics and volcani-clastics, deposited in paleo-arc basin (Metcalf 2002). Lithology of the study area consists of low-grade metamorphosed sedimentary and volcanic rocks of Gua Musang Formation of Late Permo-Triassic age (Fig. 1). The Selinsing deposit occurs along the north striking Raub Bentong Suture.

Data Used

In this study, data from two remotely sensed multispectral data were processed including Landsat 8 and ASTER level 1B thermal bands. The LANDSAT 8 image with the path 127 and row 57 was acquired on June 11, 2014 downloaded from USGS Earth explorer. ASTER data with SWIR bands have encountered problems of noise and cloud in 2008. However, the downloaded image was acquired on October 12, 2009 because the image was the least cloudy image that could be found on the Reverb website. The Level-1B

(radiance-at-sensor) data product is a re-sampled image data generated from the Level-1A data by applying the radiometric and geometric correction coefficients (Abrams 2000). Environment for Visualizing Images (ENVI 4.8) was used to analyze the images and ARCMAP 10.2 was utilized to make alteration maps and creating geological maps.

Methodology

Preprocessing of Remote Sensing Data

Figure 2 shows the methods applied on both datasets. Reflectance values from Landsat 8 bands including bands 2, 3, 4, 5, 6, 7 and emissivity (Vaughan et al. 2005) from ASTER thermal infrared Bands including 10, 11, 12, 13 and 14 were used to map key alteration minerals in the study area. After converting the DN to top of atmosphere (TOA) radiance, QUAC atmospheric correction was used to convert TOA radiance to the surface reflectance in LANDSAT 8. The quick atmospheric correction (QUAC) code performs atmospheric correction on multi- and hyperspectral imagery spanning all or part of the visible and near infrared–short wave infrared spectral range, ~ 400–2500 nm (Bernstein et al. 2012).

ASTER thermal image obtained from Reverb website was not good and unusually quite noisy as well. In order to reduce noise in data set, MNF was applied to ASTER TIR bands and inverse MNF was carried out on the first four MNF. Atmospheric Corrections available in ENVI was applied to ASTER thermal bands (Elsaid et al. 2014). This algorithm assumes that the atmosphere is uniform over the data scene and that a near-blackbody surface exists within the scene. The location of the blackbody surface is not required for this correction. A single layer approximation of the atmosphere is used. No reflected down welling radiance is also assumed (ENVI 2003).

Emissivity Retrieval

The radiance measured from the Earth’s surface in the thermal infrared consists of temperature and emissivity related to the chemistry and texture of the Earth’s surface and provide a means for mineral mapping. Unfortunately the measured radiance is dominated by surface temperature effects that mask subtle variation in emissivity. This has led to the development of a variety of techniques which either enhance or separate the emissivity from temperature information (Hook et al. 1992). In this study, Emissivity Normalization (NOR) was utilized to convert radiance to emissivity normalization methods are slightly superior to other methods such as Alpha Emissivity Method and

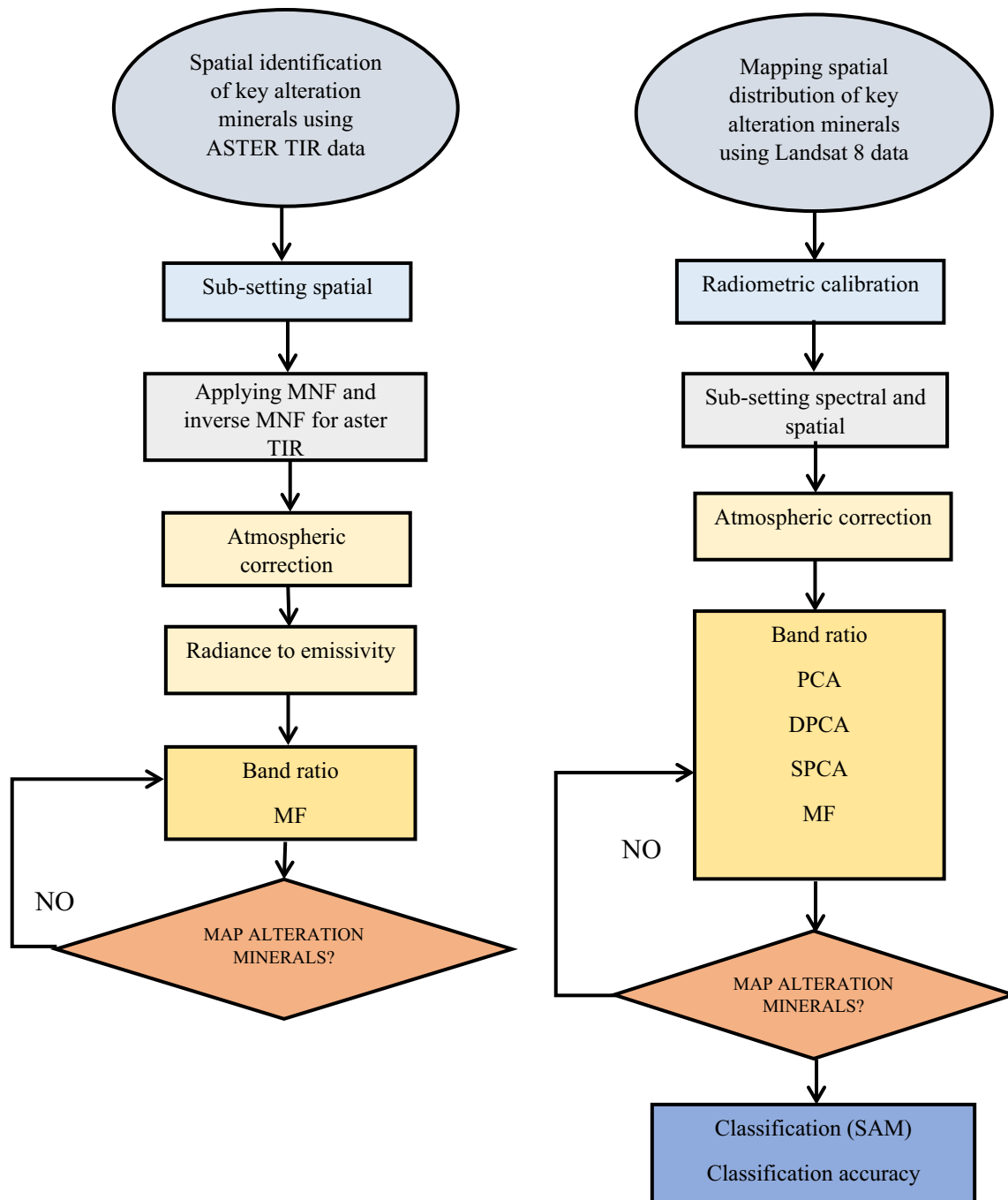


Fig. 2 Methodological flowchart applied in this study

Reference Channel Method (Li et al. 1999). This method assumes a constant emissivity in all N channels for a given pixel, which enables N temperatures to be calculated for each pixel from their radiance. The maximum of those N temperatures is considered to be the land surface temperature (T), and used to derive emissivity values for temperature (T), and used to derive emissivity values for the other channels (Hook et al. 1992).

Processing Methods

Image processing methods are based on transformation of data into image display which result in either increasing contrast between the background and interesting targets or conveying information about the composition of certain pixels in the image (Kujjo 2010). Techniques applied in this study to map clay and quartz minerals are band rationing, DPCA and MF.

Band Ratio

Band rationing is a technique where the DN value of one band is divided by the DN value of another band. Band ratios can be useful for highlighting certain features or materials that cannot be seen in the raw bands (Inzana et al. 2003). It includes mathematical operations applied to multispectral images to reduce the variations in the spectral reflectance caused by topographic or seasonal changes in sunlight illumination angle to extract specific spectral responses (Richards 1999).

Direct Principal Component Analysis (Software Defoliant Technique)

In a study area where vegetation is dense, pixels could represent purely vegetation spectra. Where vegetation is not dense enough and spatial resolution pixels is inadequate to clearly see between the trees, the pixels represent a mixture of different material. In the latter case, techniques for detection and map hydrothermally altered rocks are generally aimed at separating or reducing substantially the spectral effect of vegetation from the spectral effects of the underlying the substrate. An image enhancement technique based on principal components analysis of 2 band ratio that highlight the effect of the target of interest is known as the software defoliant technique. The input band ratio images are selected on the basis that one band ratio contains information related to component of interest (e.g. hydrothermal alteration), the spectral response of which suffers interference from the spectral response of another component (vegetation). Thus, another band ratio should contain information about this spectral component that suffers from interference. Once computed, the DPC that has loading of similar signs on both input band ratio images explains the variance due to similarities in the spectral response of the interfering component and the component of interest. The other DPC, whose loadings are of different signs on either of input band ratio images, highlights contribution unique to each of the components (Fraser and Green 1987).

Matched Filtering

MF technique performs a partial unmixing of spectra to estimate the abundance of user-defined end-members from a set of reference spectra. This technique maximizes the response of the known end-member and suppresses the response of the composite unknown background, thus matching the known signature (Harsanyi et al. 1994).

Results and Discussion

Spectral Properties

Wall rock alteration in Selinsing Gold Mine shows a direct relation with hydrothermal solution, structures, formation of quartz veins and gold mineralization. They are silicification, sericitization and argillitization. Silicification is marked by the presence of secondary quartz and sericite. Argillic alteration is indicated by the development of clay minerals such as kaolinite, muscovite and quartz. Sericitization is characterized by the formation of sericite, clay minerals, quartz, chlorite, carbon, sulphides (Hassan et al. 2008). In order to find the best bands to highlight key alteration minerals, spectral library available in ENVI 4.8 was resampled to Landsat 8 bands. Silicification, sericitization and argillitization alteration are mainly characterized by secondary Quartz, Sericite and clay minerals respectively. Clay minerals such as: Kaolinite shows AL–O–H absorption features at 2.20 and 2.17 μm , sericite has an absorption at 2.2 μm caused also by the Al–O–H bond and chlorite has absorption at 2.33 μm created by Mg–O–H bond (Fig. 3) (Rowan and Mars 2003; Yajima 2014).

Landsat 8 data has two broad bands in SWIR region, the first one (B 6) is from 1.57 to 1.65 μm and, the second one (B 7) is from 2.11 to 2.29 μm (U.S. Geological Survey 2016). Some of the OH bearing minerals (Fig. 4) have high reflectance in band 6 and low reflectance in band 7 that make Landsat 8 capable of highlighting these minerals.

The NDVI map is shown in Fig. 5. As can be seen most of the study area is covered by vegetation.

$$NDVI = (NIR - RED)/(NIR + RED) \quad (1)$$

Band Ratio

Band ratio technique is based on highlighting the spectral differences that are unique to the materials being mapped (Yetkin 2003). Kaolinite shows absorption features from 2.1 to 2.2 μm range (Band 7 of LANDSAT 8) due to molecular vibration processes becoming very prominent. Band ratio of 6/7 is expected to be high in clay minerals because they give high reflectance in band 6 and relatively low in band 7. However this ratio can be affected by vegetation due to similarity in their spectral signature in bands 6 and 7.

Based on the scatter plot of the band ratio 6/7 (X axis) and NDVI (Y axis) a pixel with vegetation cover shows high values in both ratios. Therefore pixels with vegetation cover display correlative distributions and a pixel without vegetation cover shows a high value only in the ratio of band 6 over band 7 when the rock is altered (Okada et al.

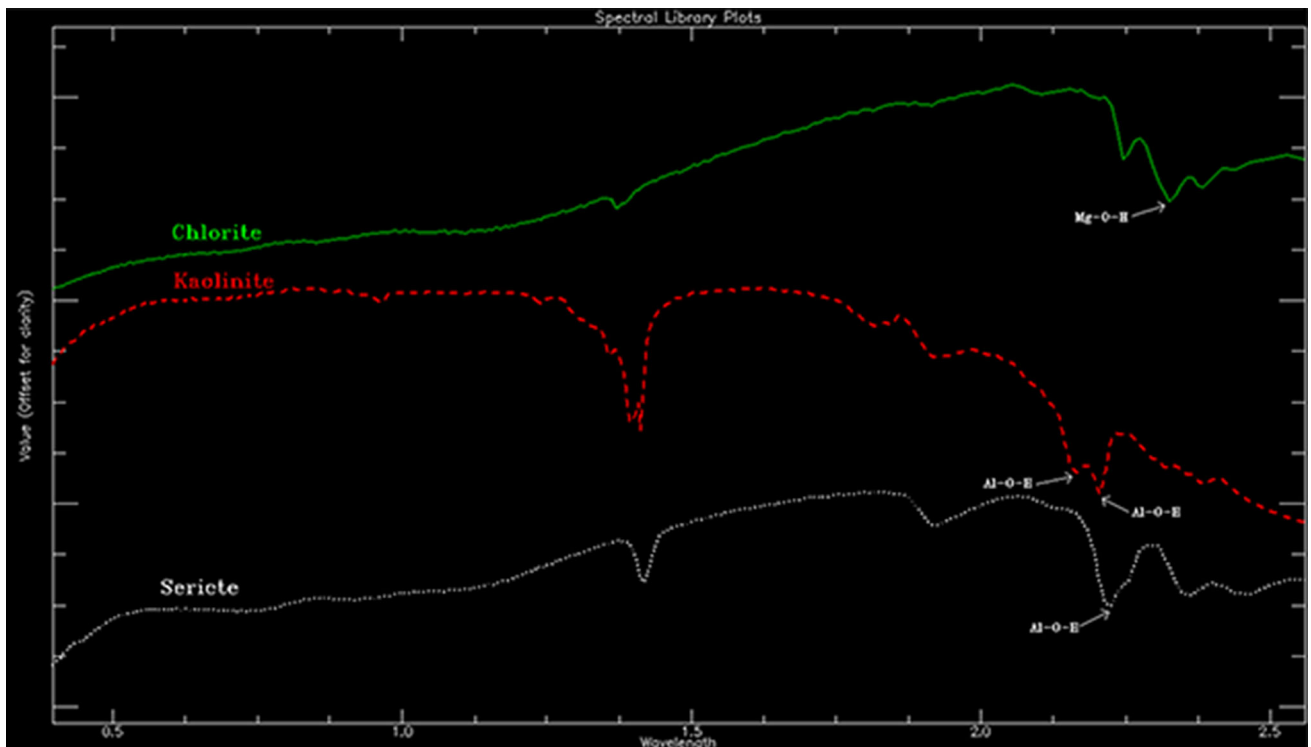


Fig. 3 Spectral signatures of Chlorite, Kaolinite and Sericite

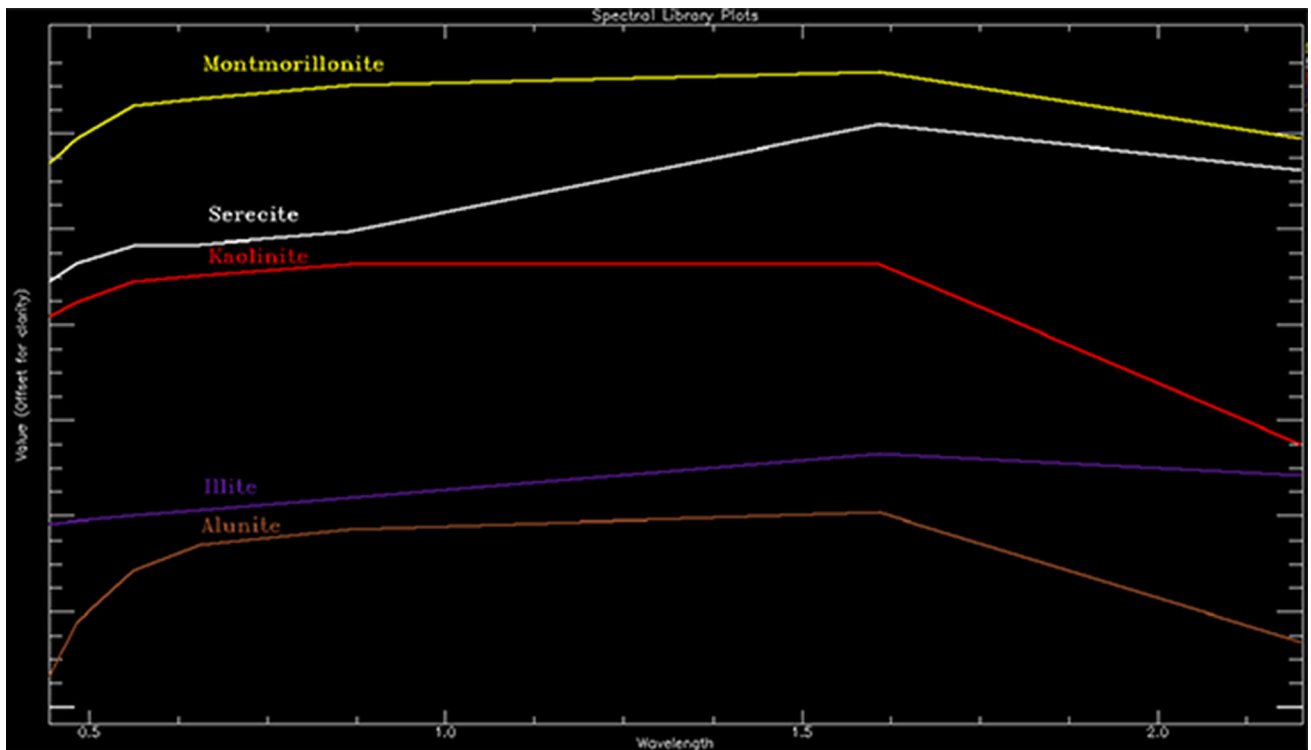


Fig. 4 Landsat 8 image showing common hydrothermal alteration minerals

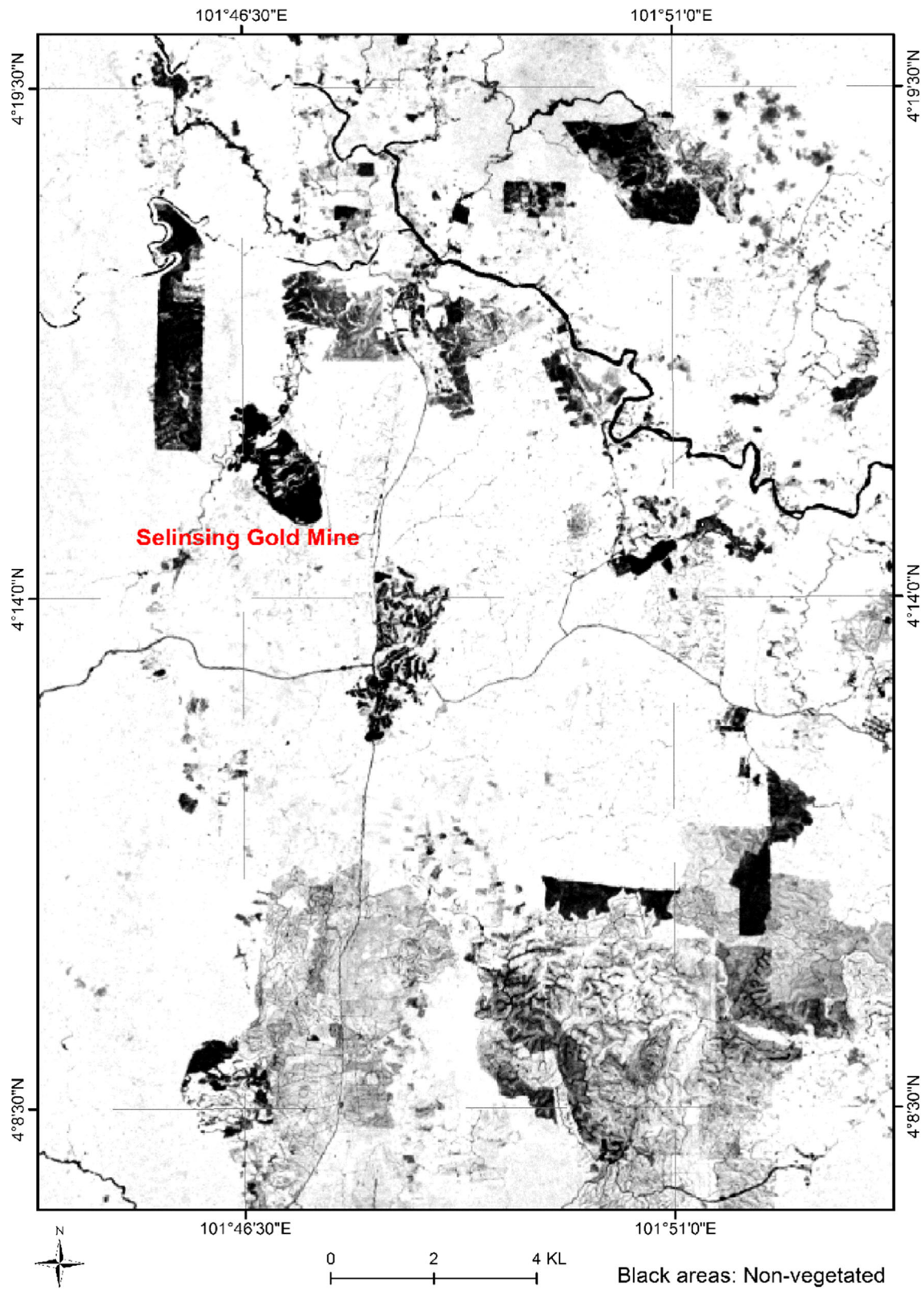
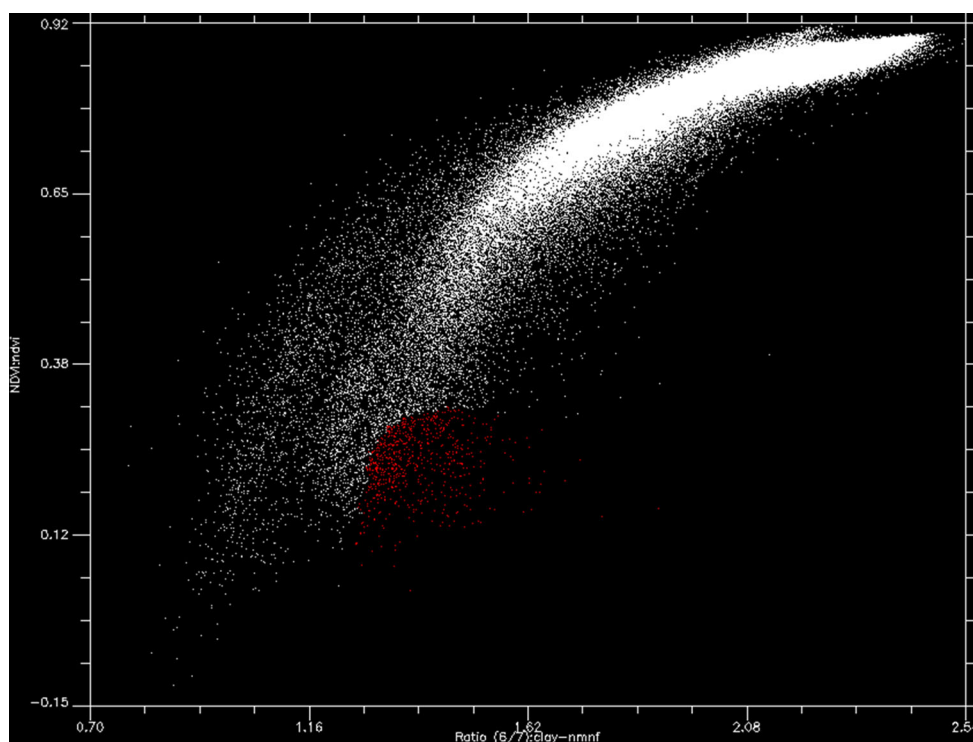


Fig. 5 Vegetated and non-vegetated areas based on NDVI

Fig. 6 Scatter plot of the NDVI and ratio 6/7 on the Y and X-axis respectively



1993). Thus, red pixels (Fig. 6) on the scatter plot could be attributed to clay minerals (Fig. 7a).

Direct Principal Component Analysis

The result of DPC analysis using band ratio 6/7 and NDVI is listed in Table 1. The first DPC is not able to make a differentiation between clay minerals and vegetation due to the similarity between eigenvalue's signs. However the second one could map clay minerals as bright pixels because of the positive sign of loading on band ratio 6/7 (Fig. 7b).

Matched Filtering

In the first step, a mask image was built based on the threshold from -0.98 to 0.45 obtained from NDVI. Next the mask image was applied to MNF image in order to show only non-vegetated areas and then Pixel Purity Index (PPI) was applied on masked MNF. N-dimensional visualization and spectral analyst were used to extract end-member which in this case is Kaolinite (Fig. 8a) and MF image was created based on the extracted end-member (Fig. 7c).

Potential Zones

The Central Belt is a highly potential region for prospecting gold exploration targets along the major lineament

structures using remote sensing technology (Pour and Hashim 2014). According to the location of known gold deposits and results of the image processing methods, prospects shown in Fig. 7d could be considered for more investigation.

Quartz Rich Zones Mapping (Band Ratio)

Quartz is one of the important rock-forming minerals that does not have diagnostic spectral absorption feature in the VNIR and SWIR regions but displays strong fundamental molecular absorption features in the TIR region ($8\text{--}12\ \mu\text{m}$) (Hunt and Salisbury 1976). Quartz shows absorption features in bands 10 and 12 of ASTER and has high emissivity in band 14 (Fig. 8b) (Ninomiya 2003). Based on above-mentioned absorption features of the Quartz, following ratio was utilized to map the areas of the high concentration of quartz (Fig. 9).

$$\text{Quartz Ratio} = \text{band14}/\text{band12} \quad (2)$$

In order to validate the results a detail fieldwork was carried out. As mentioned earlier, the wall rocks alteration in the study area are silicification, sericitization and argillitization and kaolinite, muscovite, sericite, quartz and chlorite are the major alteration minerals in the region (Hassan et al. 2008). Samples of rocks were collected from those locations in which image processing methods highlighted. In these samples, Kaolinite, alunite, sericite,

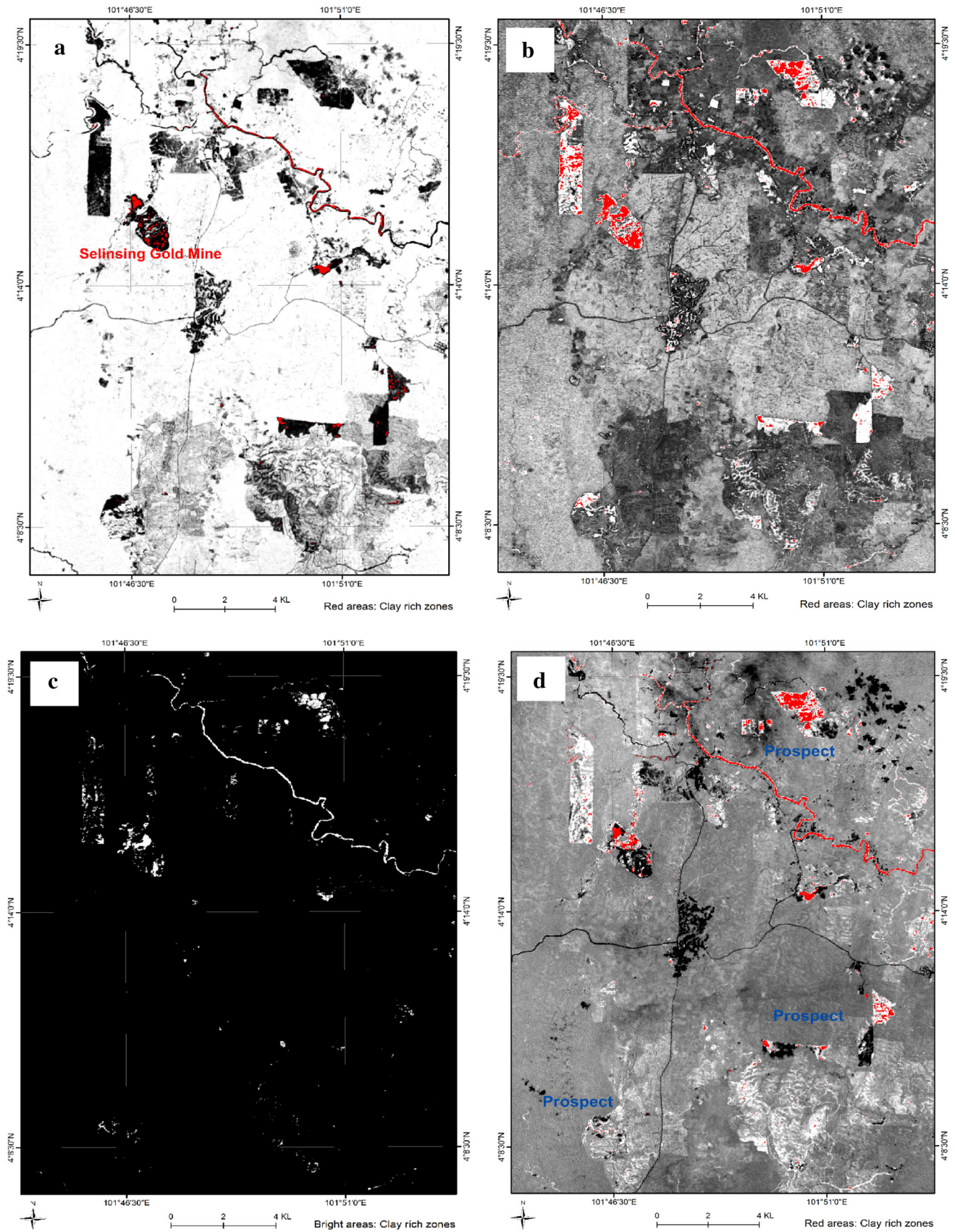


Fig. 7 Images showing clay minerals derived from a band ratio 6/7, b DPC2, c MF, and d potential areas for gold exploration zones

Table 1 Direct principle component analysis of band ratio for clay alteration

Eigenvector	NDVI	6/7
PC1	- 0.430865	- 0.902416
PC2	- 0.902416	0.430865

Bold value represent the significant values

chlorite and illite were detected by XRD analysis in the collected rock samples, thus agreeing with the finding.

Conclusion

In this paper, the application of Landsat 8 VNIR + SWIR bands and ASTER level 1B thermal bands were explored for identifying the key alteration minerals, which are associated with gold mineralization in CGB, Malaysia. Based on the in situ inspection and XRD analysis, the applied image processing methods were efficiently able to map spatial distribution of key alteration minerals in Selinsing gold mine and identified new prospects in the

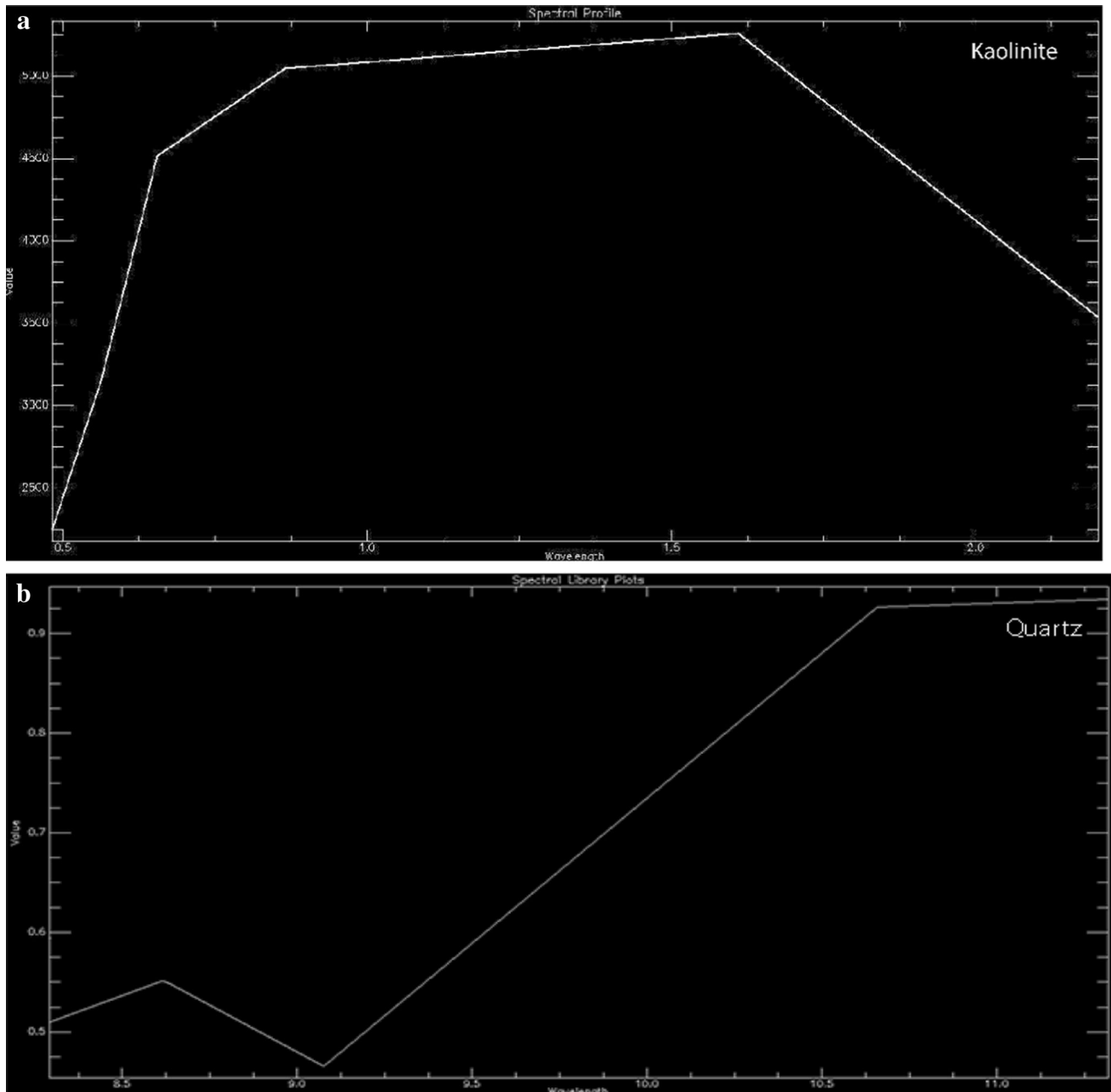


Fig. 8 **a** Spectral signature of Kaolinite extracted from image using N-dimensional visualization, and **b** represents the thermal spectral library of Quartz

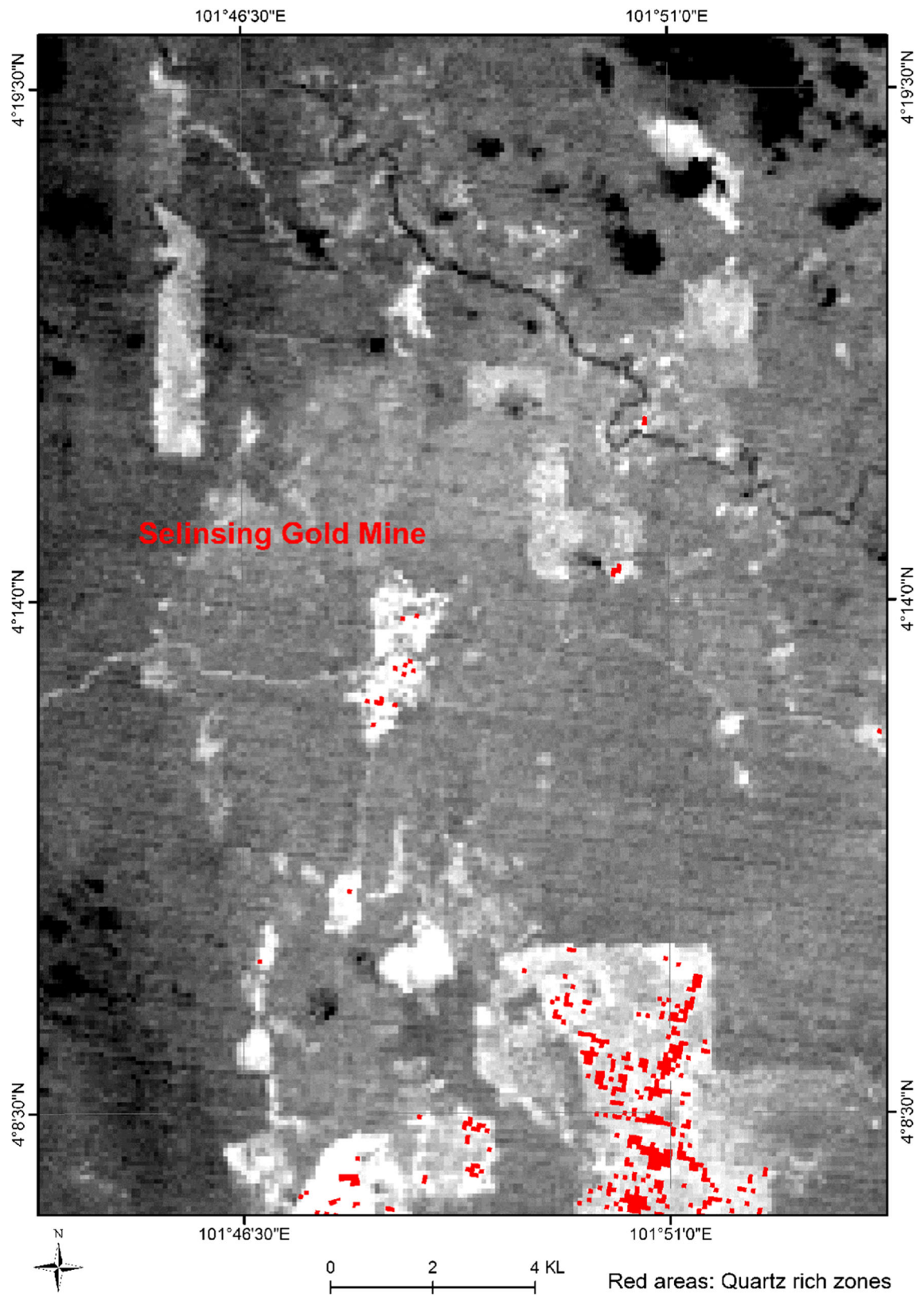


Fig. 9 Ratio 14 over 12 showing quartz rich rocks

region. The gold mineralisation has occurred in quartz veins that cut the host rocks and wall rocks with intensive alteration that are related to the N–S and NE–SW lateral faults and shear zones. Band ratio, DPCA and MF proved successful for discrimination of clay minerals using Landsat 8 bands and ASTER TIR bands were utilized to map Quartz rich zones in the study region. Band ratio 14 over 12 was carried out to highlight spatial distribution of Quartz rich zones. The results of this study show that the integration of the image processing techniques has great ability to assist economic geologists for the reconnaissance stages of mineral exploration.

Acknowledgements The authors would like to express our gratitude to the Department of Minerals and Geoscience Malaysia (JMG) for providing various essential datasets used in this study. And also to Land Processes Distributed Active Archive Center (LP DAAC) for providing ASTER L1B imagery used in this study.

References

- Abrams, M. (2000). The Advanced Spaceborne Thermal Emission and Reflection Radiometer (ASTER): Data products for the high spatial resolution imager on NASA's Terra platform. *International Journal of Remote Sensing*, 21(5), 847–859.
- Almeida-Filho, R., & Vitorello, I. (1996). Mapping of hydrothermally altered areas in vegetated terrain, using multisource data integration and segmentation techniques. *International Archives Of Photogrammetry and Remote Sensing*, 31, 7–12.
- Bernstein, L. S., Jin, X., Gregor, B., & Adler-Golden, S. M. (2012). Quick atmospheric correction code: Algorithm description and recent upgrades. *Optical Engineering*, 51(11), 111719-1.
- Boloki, M., & Poormirzaee, M. (2010). Using ASTER image processing for hydrothermal alteration and key alteration minerals mapping in Siyahrud. *Iran International Journal of Geology*, 2, 38–43.
- Campi, M. J., Shi, G. R., & Leman, M. S. (2002). The Leptodus Shales of central Peninsular Malaysia: Distribution, age and palaeobiogeographical affinities. *Journal of Asian Earth Sciences*, 20(6), 703–717.
- Chu, L. H., & Singh, D. S. (1986). The nature and potential of gold mineralization in Kelantan, Peninsular Malaysia. In *Geology of Society Malaysian Bulletin, Fifth regional Congress on geology, mineral and energy resources of Southeast Asia* (Vol. 20, pp. 431–440).
- Crosta, A. P., Sabine, C., & Taranik, J. V. (1998). Hydrothermal alteration mapping at Bodie, California, using AVIRIS hyperspectral data. *Remote Sensing of Environment*, 65(3), 309–319.
- Ducart, D. F., Crósta, A. P., Souza Filho, C. R., & Coniglio, J. (2006). Alteration mineralogy at the Cerro La Mina epithermal prospect, Patagonia, Argentina: Field mapping, short-wave infrared spectroscopy, and ASTER images. *Economic Geology*, 101(5), 981–996.
- Elsaid, M., Aboelkhair, H., Dardier, A., Hermas, E., & Minoru, U. (2014). Processing of multispectral ASTER data for mapping alteration minerals zones: As an aid for uranium exploration in Elmissikat-Eleridiya Granites, Central Eastern Desert, Egypt. *The Open Geology Journal*, 8(1), 69–83.
- ENVI User's Guide. (2003). Version 4.0.
- Feizi, F., Mansouri, E., & Ramezani, A. K. (2016). Prospecting of Au by remote sensing and geochemical data processing using fractal modelling in Shishe-Botagh, Area NW Iran. *Journal of the Indian Society of Remote Sensing*, 44(4), 539–552. <https://doi.org/10.1007/s12524-015-0510-0>.
- Fraser, S. J., & Green, A. A. (1987). A software defoliant for geological analysis of band ratios. *International Journal of Remote Sensing*, 8(3), 525–532.
- Galvao, L. S., Almeida Filho, R., Vitorello, I., Epiphanyo, J. C. N., & Fonseca, L. M. G. (2005). Use of ASTER short-wave infrared bands for the spectral discrimination of hydrothermally altered-materials: Evaluation in a tropical savannah environment. *Simpósio Brasileiro de Sensoriamento Remoto*, 12(SBSR), 1783–1788.
- Glacken, I., Blackney, P., & Murphy, M. (2006). Moncoa Corporation: Selinsing Gold Mining Project, Malaysia Project No. 5174.
- Harris, J. R., Rencz, A. N., Ballantyne, B., & Sheridan, C. (1998). Mapping altered rocks using LANDSAT TM and lithochemical data: Sulphurets-Brucejack Lake district, British Columbia, Canada. *Photogrammetric Engineering and Remote Sensing*, 64(4), 309–322.
- Harsanyi, J. C., Farrand, W., & Chang, C. I. (1994). Detection of subpixel spectral signatures in hyperspectral image sequences. In *Annual meeting, proceedings of American Society of Photogrammetry & Remote Sensing* (pp. 236–247).
- Hassan, W. F. W., Basori, M. B. I., & Abdullah, I. (2008). Perubahan batuan dinding yang berkaitan dengan pemineralan emas di Selinsing Gold Mine, Pahang [Wall rock alteration related to gold mineralisation in Selinsing Gold Mine, Pahang]. *Bulletin of the Geological Society of Malaysia*, 54, 75–80.
- Hook, S. J., Gabell, A. R., Green, A. A., & Kealy, P. S. (1992). A comparison of techniques for extracting emissivity information from thermal infrared data for geologic studies. *Remote Sensing of Environment*, 42(2), 123–135.
- Hosseinjani Zadeh, M., Tangestani, M. H., Roldan, F. V., & Yusta, I. (2014). Sub-pixel mineral mapping of a porphyry copper belt using EO-1 Hyperion data. *Advances in Space Research*, 53(3), 440–451.
- <http://landsat.usgs.gov>. U.S. Geological Survey. U.S. Department of the Interior; Updated 2016 Jan 16.
- Hunt, G. R., & Salisbury, J. W. (1976). *Mid-infrared spectral behavior of metamorphic rocks*. Environmental Research Papers Air Force Cambridge Research Labs.
- Inzana, J., Kusky, T., Higgs, G., & Tucker, R. (2003). Supervised classifications of Landsat TM band ratio images and Landsat TM band ratio image with radar for geological interpretations of central Madagascar. *Journal of African Earth Sciences*, 37(1), 59–72.
- Iswadi, M. B., Abdullah, I., & Fuad, W. H. (2009). The relationships of structure and deformation to the gold mineralization in Selinsing Gold Mine, Pahang. *Geological Society of Malaysia Bulletin*, 55, 33–37.
- Kujjo, G. P. (2010). *Application of remote sensing for gold exploration in the Nuba Mountains, Sudan*. Doctoral dissertation: Bowling Green State University.
- Lee, A. K., & Sallehuddin, M. (1990). *Orientation study on sampling density using heavy mineral stream concentrates for reconnaissance gold exploration in the Selinsing area, Pahang darul Makmur*. Proceedings of the 21st Geological Conference. p. 33.
- Li, Z. L., Becker, F., Stoll, M. P., & Wan, Z. (1999). Evaluation of six methods for extracting relative emissivity spectra from thermal infrared images. *Remote Sensing of Environment*, 69(3), 197–214.
- Makoundi, C. (2012). *Geology, geochemistry and metallogenesis of selected sediment-hosted gold deposits in the Central Gold Belt, Peninsular Malaysia*. Doctoral dissertation: University of Tasmania.

- Metcalfe, I. (1986). Late Palaeozoic palaeogeography of Southeast Asia: Some stratigraphical, palaeontological and palaeomagnetic constraints. *Geological Society of Malaysia Bulletin*, 19, 153–164.
- Metcalfe, I. (1988). Origin and assembly of south-east Asian continental terranes. *Geological Society, London, Special Publications*, 37(1), 101–118.
- Metcalfe, I. (2000). The Bentong–Raub suture zone. *Journal of Asian Earth Sciences*, 18(6), 691–712.
- Metcalfe, I. (2002). Permian tectonic framework and palaeogeography of SE Asia. *Journal of Asian Earth Sciences*, 20(6), 551–566.
- Molan, Y. E., Refahi, D., & Tarashti, A. H. (2014). Mineral mapping in the Maherabad area, eastern Iran, using the HyMap remote sensing data. *International Journal of Applied Earth Observation and Geoinformation*, 27, 117–127. <https://doi.org/10.1016/j.jag.2013.09.014>.
- Moore, F., Rastmanesh, F., Asadi, H., & Modabberi, S. (2008). Mapping mineralogical alteration using principal-component analysis and matched filter processing in the Takab area, north-west Iran, from ASTER data. *International Journal of Remote Sensing*, 29(10), 2851–2867.
- Ninomiyama, Y. (2003). A stabilized vegetation index and several mineralogical indices defined for ASTER VNIR and SWIR data. In *Geoscience and remote sensing symposium, 2003. IGARSS'03. Proceedings. 2003 IEEE international* (Vol. 3, pp. 1552–1554).
- Okada, K., Segawa, K., & Hayashi, I. (1993). Removal of the vegetation effect from LANDSAT TM and GER imaging spectroradiometer data. *ISPRS Journal of Photogrammetry and Remote Sensing*, 48(6), 16–27.
- Oskouei, M. M., & Babakan, S. (2016). Detection of alteration minerals using hyperion data analysis in Lahroud. *Journal of the Indian Society of Remote Sensing*, 44(5), 713–721.
- Pour, A. B., & Hashim, M. (2011). Identification of hydrothermal alteration minerals for exploring of porphyry copper deposit using ASTER data, SE Iran. *Journal of Asian Earth Sciences*, 42(6), 1309–1323.
- Pour, A. B., & Hashim, M. (2014). Integrating PALSAR and ASTER data for mineral deposits exploration in tropical environments: A case study from Central Belt, Peninsular Malaysia. *International Journal of Image and Data Fusion*. <https://doi.org/10.1080/19479832.2014.985619>.
- Pour, A. B., & Hashim, M. (2015). Hydrothermal alteration mapping from Landsat-8 data, Sar Cheshmeh copper mining district, south-eastern Islamic Republic of Iran. *Journal of Taibah University for Science*, 9(2), 155–166.
- Pour, A. B., Hashim, M., & van Genderen, J. (2013). Detection of hydrothermal alteration zones in a tropical region using satellite remote sensing data: Bau goldfield, Sarawak, Malaysia. *Ore Geology Reviews*, 54, 181–196. <https://doi.org/10.1016/j.oregeorev.2013.03.010>.
- Richards, J. A. (1999). *Remote sensing digital image analysis* (Vol. 3). Berlin: Springer.
- Rowan, L. C., Hook, S. J., Abrams, M. J., & Mars, J. C. (2003). Mapping hydrothermally altered rocks at Cuprite, Nevada, using the Advanced Spaceborne Thermal Emission and Reflection Radiometer (ASTER), a new satellite-imaging system. *Economic Geology*, 98(5), 1019–1027.
- Rowan, L. C., & Mars, J. C. (2003). Lithologic mapping in the Mountain Pass, California area using advanced spaceborne thermal emission and reflection radiometer (ASTER) data. *Remote Sensing of Environment*, 84(3), 350–366.
- Salisbury, J. W., Wald, A., & D'Aria, D. M. (1994). Thermal-infrared remote sensing and Kirchhoff's law: I. Laboratory measurements. *Journal of Geophysical Research: Solid Earth*, 99, 11897–11911. <https://doi.org/10.1029/93JB03600>.
- Vaughan, R. G., Hook, S. J., Calvin, W. M., & Taranik, J. V. (2005). Surface mineral mapping at Steamboat Springs, Nevada, USA, with multi-wavelength thermal infrared images. *Remote Sensing of Environment*, 99(1), 140–158.
- Volesky, J. C., Stern, R. J., & Johnson, P. R. (2003). Geological control of massive sulfide mineralization in the Neoproterozoic Wadi Bidah shear zone, southwestern Saudi Arabia, inferences from orbital remote sensing and field studies. *Precambrian Research*, 123(2–4), 235–247. [https://doi.org/10.1016/S0301-9268\(03\)00070-6](https://doi.org/10.1016/S0301-9268(03)00070-6).
- Yajima, T. (2014). *ASTER data analysis applied to mineral resource exploration and geological mapping*. Doctorate dissertation: Nagoya University.
- Yetkin, E. (2003). *Alteration mapping by remote sensing: Application to Hasandag–Melendiz volcanic complex*. Doctorate dissertation: Middle East Technical University.